Available online at www.sciencedirect.com

ScienceDirect

Advances in Space Research 68 (2021) 1864–1875

ADVANCES IN SPACE RESEARCH
(a COSPAR publication)

www.elsevier.com/locate/asr

A mechanism for electrostatic solitary waves observed in the reconnection jet region of the Earth's magnetotail

G.S. Lakhina [a,*], S.V. Singh [a], R. Rubia [b]

[a] Indian Institute of Geomagnetism Navi Mumbai, 410218, India
[b] P-12/14 Tarapore Enclave, Rangpuri, New Delhi 110070, India

Received 16 February 2021; received in revised form 13 April 2021; accepted 15 April 2021
Available online 24 April 2021

Abstract

Electrostatic solitary waves (ESWs) have been observed in the reconnection jet region in the Earth's magnetotail by the Magnetospheric Multiscale spacecraft (MMS). A mechanism for the reconnection jet ESWs is proposed in terms of slow and fast ion-acoustic solitons. At the time of occurrence of ESWs, no hot plasmasheet ions were observed. Based on the observations, the reconnection jet plasma is modeled by a three-component magnetized plasma consisting of hot electrons and two cold ion beams streaming parallel and anti-parallel to the magnetic field, **B** respectively. The model is based on the Sagdeev pseudopotential technique, and it predicts four types of ion-acoustic solitons, namely, two fast and two slow ion-acoustic solitons, where one of each type propagates parallel and another anti-parallel to the ambient magnetic field, respectively. The theoretical model predicts bipolar electric fields with amplitudes in the range of $\approx$ (3–69) mV m^{-1}, positive potentials with amplitudes of $\approx$ (51–539) V, and the soliton widths of $\approx$ (4.5–10.3) Debye lengths. These predictions are in good agreement with the observed characteristics of ESWs in the reconnection jet region.
© 2021 COSPAR. Published by Elsevier B.V. All rights reserved.

Keywords: Electrostatic solitary structures; Magnetic reconnection; Waves in reconnection jets; Ion-acoustic solitons; Plasma waves and instabilities

1. Introduction

Matsumoto et al. (1994) were the first to report the existence of electrostatic solitary waves (ESWs) in the plasma sheet boundary layer. Later on, they were observed in several regions of the Earth's magnetosphere (Franz et al., 1998; Tsurutani et al., 1998; Bale et al., 1998; Ergun et al., 1998a; Bounds et al., 1999; Pickett et al., 2003; Pickett et al., 2004; Pickett et al., 2005; Mozer et al., 2015). ESWs are nonlinear electrostatic solitary structures observed in the parallel electric fields and are usually bipolar or tripolar. ESWs can have either positive potentials (electron holes) or negative potentials (ion holes), and generally their amplitudes decrease with distance from the Earth. For example, ESWs amplitudes vary from 100s mV m^{-1} in auroral region to fraction of a mV m^{-1} in the plasma sheet boundary layer (Matsumoto et al., 1994; Kojima et al., 1997; Ergun et al., 1998b; Omura et al., 1999; Pickett et al., 2004; Franz et al., 2005; Norgren et al., 2015). Similarly, both the velocities and parallel scale sizes of ESWs vary substantially with the distance from the Earth, e.g., going from the auroral region to the plasma sheet boundary layer, the velocities and parallel scale sizes of ESWs could vary from $\sim$ a few 100 km s^{-1} to a few 10000 km s^{-1}, and from $\sim$ 100 m to several 10s km, respectively(Cattell et al., 1999; Omura et al., 1999). It is noticed that fast ESWs, with speeds greater than ion acoustic speed and close to electron thermal speed, are generally associated with high speed electron beams. Such ESWs are interpreted to be either phase space electron

* Corresponding author.
E-mail addresses: gslakhina@gmail.com, gurbax.lakhina@iigm.res.in (G.S. Lakhina).

https://doi.org/10.1016/j.asr.2021.04.026
0273-1177/© 2021 COSPAR. Published by Elsevier B.V. All rights reserved.

holes (Bernstein et al., 1957; Schamel, 1982; Singh and Schunk, 1984; Singh et al., 1987; Omura et al., 1996; Kojima et al., 1997; Muschietti et al., 1999; Goldman et al., 1999; Jovanović and Shukla, 2000; Singh et al., 2001a; Drake et al., 2003; Singh and Khazanov, 2003; Pickett et al., 2003; Chen et al., 2005; Che et al., 2010; Hutchinson, 2017) or electron acoustic solitary waves (Pottelette et al., 1990; Pottelette et al., 1999; Dubouloz et al., 1991; Dubouloz et al., 1993; Berthomier et al., 1998; Berthomier et al., 2000; Singh et al., 2001b; Singh and Lakhina, 2001; Singh and Lakhina, 2004; Tagare et al., 2004; Cattaert et al., 2005; Kakad et al., 2007; Ghosh et al., 2008; Lakhina et al., 2008a; Lakhina et al., 2008b; Lakhina et al., 2009; Lakhina et al., 2011; Singh et al., 2011; Maharaj et al., 2012a). On the other hand, the slow ESWs, with speeds close to ion acoustic speed/ion thermal speed, are generally found to be associated with ion beams. Slow ESWs have been interpreted either as phase space ion holes (Temerin et al., 1982; Boström et al., 1988; Koskinen et al., 1990; Bounds et al., 1999) or ion-acoustic solitary waves (Koskinen et al., 1990; Hudson et al., 1983; Reddy and Lakhina, 1991; Reddy et al., 1992; Maharaj et al., 2012b; Singh et al., 2013; Mahmood and Ur-Rehman, 2013; Ur-Rehman et al., 2014; Maharaj et al., 2015; Rufai et al., 2015). Recently, slow electron holes have been observed in the plasma sheet boundary layer (Norgren et al., 2015), and at the reconnection site (Khotyaintsev et al., 2010; Graham et al., 2015). Kakad et al. (2016) have proposed that slow ion-acoustic solitons can explain main characteristics of the slow electron holes observed in the plasma sheet boundary layer (Norgren et al., 2015).

Magnetic reconnection is considered as a fundamental plasma process that can convert magnetic energy into plasma kinetic energy accompanied by changes in the magnetic topology (Giovanelli, 1947; Dungey, 1961; Vasyliunas, 1975; Lakhina, 2000; Angelopoulos et al., 2008; Birn and Hesse, 2014; Fu et al., 2017; Yamada et al., 2010). During magnetic reconnection process, initially two isolated plasmas become magnetically connected, and the reconnected plasmas are ejected with high speeds from the reconnection outflow region. Such high-speed plasma outflows are called as reconnection jets or bursty bulk flows (Angelopoulos et al., 1992; Cao et al., 2006; Cao et al., 2013). It has been proposed that reconnection jets can play an important role in plasma energization in space plasmas (Khotyaintsev et al., 2011; Fu et al., 2011; Lapenta et al., 2014; Lu et al., 2016; Liu et al., 2017; Zhou et al., 2018; Sitnov et al., 2019; Chen et al., 2019; Zhao et al., 2019), solar flares (Shibata et al., 1995), and in high-energy astrophysical context, e.g., pulsar winds (Kirk and Skjaeraasen, 2003), active galactic nuclei (Larrabee et al., 2003) and gamma-ray bursts (GRBs) (Drenkhahn and Spruit, 2002), etc.

Reconnection jets in the Earth's magnetotail can support a variety of plasma waves and instabilities, like, whistler instability (Deng et al., 2010; Khotyaintsev et al., 2011; Huang et al., 2012; Fu et al., 2014), lower hybrid instability (Khotyaintsev et al., 2011; Divin et al., 2017; Liu et al., 2018a; Liu et al., 2018b; Pan et al., 2018), broadband high-frequency waves (Hwang et al., 2014; Yang et al., 2017), and electrostatic solitary waves (ESWs)(Deng et al., 2010; Ergun et al., 2014; Liu et al., 2019). ESWs have been observed not only in the reconnection jets (Deng et al., 2010; Ergun et al., 2014; Liu et al., 2019), but at the separatrices (Huang et al., 2014; Wang et al., 2014; Graham et al., 2015) and inside magnetic flux ropes (Khotyaintsev et al., 2010) associated with magnetic reconnection. Recently, Liu et al. (2019) have analyzed the high-cadence data from the Magnetospheric Multiscale (MMS) spacecraft, and reported the first observational evidence of ESWs generation by accelerated cold ion beams inside the reconnection jet. The reconnection jet region was found to have two counterstreaming ion (proton) beams and hot electrons. The ion beams have a maximum relative speed of $\sim$ 2000 km s^{-1} at the time of the ESWs. During the occurrence of ESWs neither strong currents nor the hot ions (with temperature of $\sim$10 keV or so which are usually present in the magnetotail) were observed. The ESWs were found to have amplitudes up to 30 mV m^{-1}. Based on their linear instability analysis, Liu et al. (2019) suggested that ion beams can be a source of free energy for the ESWs.

In this paper, we apply a three-component fluid plasma model consisting of hot Maxwellian electrons, and two counterstreaming ion beams, developed by Lakhina et al. (2020), to explain the occurrence of ESWs observed in the reconnection jets in terms of slow and fast ion-acoustic solitons. Since the observed temperatures of beam ions are smaller than that of electrons, the ion-acoustic modes can exist in this system. We would like to point out that the model discussed here deals with the time-stationary state of the plasma system when the plasma instabilities excited by the counterstreaming ion beams have saturated. This model deals essentially with the nonlinear modes of the system. In Section 2, we briefly summarize the observations of reconnection jet ESWs reported by Liu et al. (2019). Section 3, describes the theoretical model. Section 4 discusses the application of the model to reconnection jet ESWs. Section 5 gives the summary.

2. Observations

Fig. 1 illustrates an overview of MMS1 observations during the reconnection jet front (JF) crossing (Liu et al., 2019). The data are presented in **NML** coordinates, which are derived from the minimum variance analysis of **B** during the JF crossing. Here **N** is normal to the JF, **L** is approximately parallel to **B**, and **M** completes the right-handed **NML** system (Liu et al.. 2019). The jet front/dipolarization front is associated with rapid increase in the near parallel magnetic field component, B_L (Fig. 1a), decline in electron density (Fig. 1b) and intense electric fields (Fig. 1c and 1d). Fig. 1c shows the perpendicular electric

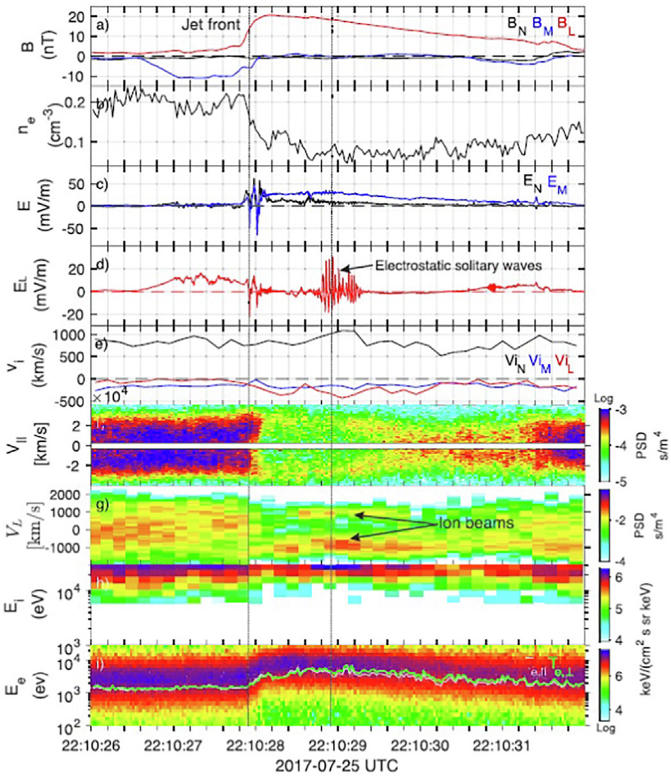

Fig. 1. An overview of MMS1 observations during JF crossing: (a) magnetic field, (b) electron density, (c) perpendicular electric field components (E_M and E_N), (d) parallel electric field component ($E_L \sim E_{\|}$), (e) ion velocity, (f) electron phase space velocity in the parallel direction. However, there is a large uncertainty in the measurements of low energy <100 eV electrons, and they are excluded, (g) ion phase space velocity in the near parallel direction (V_L), (h) ion energy spectrum, and (i) electron energy spectrum. Reprinted from Liu et al., ''Ion–beam driven intense electrostatic solitary waves in reconnection jet'', Geophys. Res. Lett., 46 [2019].

field components E_N and E_M, and Fig. 1d shows the near parallel electric field components, E_L, having bipolar structure corresponding to ESWs. The perpendicular components of the intense electric field are predominant and has a spiky aspect owing to the ripples generated by density gradient driven lower hybrid drift instability. Fig. 1e shows the ion velocity. The JF crossing is associated with sharp changes in the electron and ion distributions. Fig. 1f depicts the electron 1-D reduced distribution function in terms of electron phase space velocity in the parallel direction to **B** ($V_{\|}$). Across the JF electrons are rarer and hotter and have no field aligned beams. Fig. 1g shows the ion 1-D reduced distribution in terms of ion phase space velocity in the near parallel direction to **B** (V_L). The ion distribution function transforms from nearly flattop to counterstreaming distribution. The abrupt changes are also evident from the ion (Fig. 1h) and electron energy spectrogram (Fig. 1i). It should be noted that in Fig. 1h, the energy spectrum is dominated by the ion beam flow energy rather than their thermal energy (Liu et al., 2019). Figs. 2f-h of Liu et al. (2019), which are 2-D reduced ion distribution functions

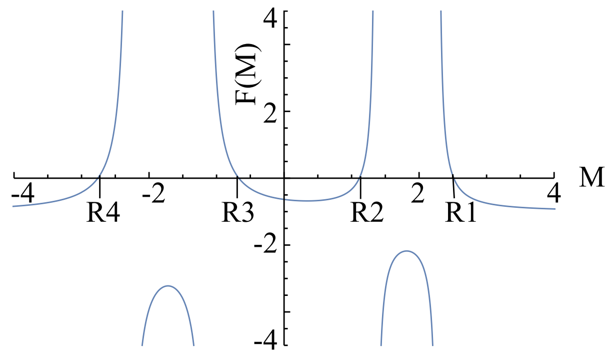

Fig. 2. Variation of $F(M)$, the second derivative of the Sagdeev pseudopotential $S(\phi, M)$ at $\phi = 0$, *versus* the Mach number M for the normalized reconnection jet plasma parameters: $n_1^0 = 0.74$, $n_2^0 = 0.26$, $\sigma_1 = 0.11$, $\sigma_2 = 0.07$, $U_1 = -1.72$ and $U_2 = 1.82$. There are four real roots (R1, R2, R3 and R4) giving critical Mach numbers for two fast ion-acoustic (R1 and R4) modes, and two slow ion-acoustic (R2 and R3) modes.

in **L**- **N** plane, clearly show two counterstreaming cold ion beams at the time of ESWs. The cold ion beams have similar speed in the **N** direction, which is close to jet speed of ~ 1200 km s^{-1}, but propagate in opposite directions along **L** (or field-aligned direction) with a maximum relative drift speed approaching ~ 2000 km s^{-1}. The average flow energy of the beam ions is, therefore, ~ 12.5 keV whereas their thermal energy is ~ 300 eV or less (Liu et al., 2019). This indicates that the ion spectrum in Fig. 1h is predominantly due to ion flow energy. This rules out the presence of hot plasma sheet ions with temperature of ~ 10 keV in the reconnection jet. The electrons get heated and accelerated inside the flux pileup region (Fig. 1i). The localized intense short duration parallel electric fields ($E_{\|} \sim E_L$) (Fig. 1d) are interpreted as ESWs as they have an asymmetric bipolar profile and broadband power spectrogram (not depicted). No signature of an electron beam (Fig. 1f) was found to be associated with the ESWs signifying that electron beam instability does not play a role in the generation of ESWs. However, two counter streaming cold ion beams (Fig. 1g) are found in the field aligned direction indicating that the ESWs are generated by ion beams.

Since the ESWs are observed by all four MMS spacecraft, Liu et al. (2019) used timing analysis and calculated the velocity of ESWs to be $\mathbf{V}_{ESW}$ = 820 * [-0.06, 0.60, 0.79] km s^{-1}, which is comparable to the local ion thermal speed and antiparallel to the local magnetic field, **B**. The ESWs were found to be positive potential structures (or electron holes), their electric field amplitudes vary from ~ a few mV m^{-1} up to 30 mV m^{-1}, and their length scale (W) were ~ 9.5 λ_D, where λ_D is the local Debye length. From the ion 2-D reduced velocity distributions (cf. Figs. 2f-h of Liu et al. (2019)) at the time of ESWs, Liu et al. (2019) deduced the ion parameters as: density of proton beam 1, N_1 =0.026 cm^{-3}, temperature of proton beam 1, T_1 = 300 eV, streaming speed of proton beam 1 anti-parallel to **B**, V_1 = −900 km s^{-1}, density of proton beam 2, N_2

=0.009 cm^{-3}, temperature of proton beam 2, T_2 =200 eV, streaming speed of proton beam 2 parallel to **B**, V_2 = 950 km s^{-1}. The electron temperature deduced from Fig. 1i is T_e =2.86 keV. The electron density, as deduced from the charge neutrality condition, is N_e =N_1+N_2= 0.035 cm^{-3}. However, this value of electron density is about half of the average N_e observed at the time of ESWs (see Fig. 1b). This indicates a possibility of some undetected ion density, e.g., background protons or oxygen ion beams as assumed by Liu et al. (2019). Further, Liu et al. (2019) performed a linear analysis of the system with above parameters, and it was found that the system is unstable to ion beam instability. However, the phase velocities of the unstable waves were one fourth of V_{ESW}, the observed speed of the ESWs. Including counterstreaming oxygen ion beams in the analysis yielded the wave phase velocities more closer to the observed V_{ESW}. However, it should be mentioned that oxygen ion beams were not actually observed in the reconnection jet at the time of ESWs occurrence.

3. Ion-acoustic soliton model

The reconnection jet plasma is modeled by an infinite, collisionless and magnetized plasma system consisting of three components, namely, hot Maxwellian electrons with density, N_e and temperature, T_e, and two fluid proton beams with densities N_1 and N_2, temperatures T_1 and T_2, and beam speeds along the ambient magnetic field, **B**= B **x**, as V_1 and V_2, respectively. The subscripts 1 and 2 refer to the parameter of proton beam 1 and proton beam 2, respectively. To maintain charge neutrality in the equilibrium state, we take $N_e = N_1 + N_2$. We consider the electrostatic waves propagating parallel to the magnetic field **B**.

The normalized number density of hot Maxwellian electrons in the presence of ion-acoustic waves with potential ϕ can be written as (Lakhina et al., 2014; Lakhina et al., 2020)

$$n_e = exp(\phi) \tag{1}$$

The dynamics of the proton beams is governed by the multifluid equations of continuity, momentum, equation of state of each species, and the Poisson equation (Lakhina et al., 2018):

$$\frac{\partial n_j}{\partial t} + \frac{\partial (n_j v_j)}{\partial x} = 0, \tag{2}$$

$$\frac{\partial v_j}{\partial t} + v_j \frac{\partial v_j}{\partial x} + \frac{1}{n_j}\frac{\partial P_j}{\partial x} + \frac{\partial \phi}{\partial x} = 0, \tag{3}$$

$$\frac{\partial P_j}{\partial t} + v_j \frac{\partial P_j}{\partial x} + 3P_j \frac{\partial v_j}{\partial x} = 0, \tag{4}$$

$$\frac{\partial^2 \phi}{\partial x^2} = (n_e - n_1 - n_2). \tag{5}$$

Here, the subscript $j = 1$ and 2 for the proton beams 1 and 2, respectively, and the adiabatic index $\gamma_j = 3$ is taken in Eq. (4). The number densities are normalized by the equilibrium number density of electrons, $N_0 = N_e = N_1 + N_2$, velocities are normalized with the ion-acoustic speed, $C_a = \sqrt{T_e/m_p}$; m_p is the mass of the proton, lengths are normalized with the electron Debye length, $\lambda_{De} = \sqrt{T_e/4\pi N_0 e^2}$; e is the electronic charge, time is normalized with the inverse of the proton plasma frequency, $\omega_{pp} = \sqrt{4\pi N_0 e^2/m_p}$ and electrostatic potential, ϕ is normalized with T_e/e, and the thermal pressure P_j with $N_e T_e$. Similarly, $\sigma_j = T_j/T_e$, $n_j^0 = N_j/N_0$ and $U_j = V_j/C_a$ are the normalized temperature, equilibrium number density, and drift speed of the jth species.

In order to investigate the properties of arbitrary amplitude ion-acoustic solitons, we transform the above set of Eqs. (2)–(5) to a stationary frame moving with velocity V, the phase velocity of the electrostatic solitary wave, i.e., $\xi = (x - Mt)$, where $M = V/C_a$ is the Mach number.

Then, solving for perturbed proton beam densities, putting these expressions in the Poisson equation, and assuming appropriate boundary conditions for the localized disturbances along with the conditions that the electrostatic potential $\phi = 0$, and $d\phi/d\xi = 0$ at $\xi \to \pm\infty$, we get the following energy integral (Lakhina et al., 2014; Lakhina et al., 2018; Lakhina et al., 2020):

$$\frac{1}{2}\left(\frac{d\phi}{d\xi}\right)^2 + S(\phi, M) = 0 \tag{6}$$

Eq. (6) describes the motion of a pseudo-particle of unit mass in a pseudopotential $S(\phi, M)$, where, ϕ and ξ play the role of displacement from the equilibrium and time, respectively. The Sagdeev pseudopotential, $S(\phi, M)$, is given by (Rubia et al., 2017; Rubia et al., 2018; Lakhina et al., 2018; Lakhina et al., 2020)

$$\begin{aligned} S(\phi,M) = \; & [1 - \exp\phi] \\ + \; & \frac{n_1^0}{6\sqrt{3\sigma_1}}\Big\{\left(M - U_1 + \sqrt{3\sigma_1}\right)^3 \\ - \; & \left[\left(M - U_1 + \sqrt{3\sigma_1}\right)^2 - 2\phi\right]^{3/2} \\ - \; & \left(M - U_1 - \sqrt{3\sigma_1}\right)^3 \\ + \; & \left[\left(M - U_1 - \sqrt{3\sigma_1}\right)^2 - 2\phi\right]^{3/2}\Big\} \\ + \; & \frac{n_2^0}{6\sqrt{3\sigma_2}}\Big\{\left(M - U_2 + \sqrt{3\sigma_2}\right)^3 \\ - \; & \left[\left(M - U_2 + \sqrt{3\sigma_2}\right)^2 - 2\phi\right]^{3/2} \\ - \; & \left(M - U_2 - \sqrt{3\sigma_2}\right)^3 \\ + \; & \left[\left(M - U_2 - \sqrt{3\sigma_2}\right)^2 - 2\phi\right]^{3/2}\Big\} \end{aligned} \tag{7}$$

Please note that Eq. (7) is written in symbolic form where the operation of a square root on a squared expression returns the same expression, e.g., $\sqrt{(M \pm \sigma_j)^2}$=$(M \pm \sigma_j)$. Please note that in the absence of drift speed of proton beams, i.e., U_1=U_2=0, the results of Lakhina et al. (2014) and Rubia et al. (2016) (in the limit $\kappa \to \infty$) can be obtained.

Eq. (6) gives a soliton solution when the pseudoparticle gets reflected in the pseudopotential field and returns to its initial state (zero potential drop) (Lakhina et al., 2011). Then, for the existence of soliton solutions, the Sagdeev pseudopotential $S(\phi, M)$ must satisfy the following conditions: (i) $S(\phi, M) = 0$, $dS(\phi, M)/d\phi$=0, and $d^2S(\phi, M)/d\phi^2$ <0 at $\phi = 0$, (ii) $S(\phi, M)$=0 at $\phi = \phi_0$ (ϕ_0 is the amplitude of the soliton), and (iii) $S(\phi, M)$ <0 for $0 < |\phi| < |\phi_0|$.

The Sagdeev pseudopotential, $S(\phi, M)$ given by Eq. (7) and its first derivative with respect to ϕ vanish at $\phi = 0$. Defining $F(M)$= $d^2S(\phi, M)/d\phi^2$at $\phi = 0$, we have

$$F(M) = \frac{n_1^0}{[(M - U_1)^2 - 3\sigma_1]} + \frac{n_2^0}{[(M - U_2)^2 - 3\sigma_2]} - 1$$

The soliton condition demands that $F(M)$ <0 must be satisfied. The critical Mach numbers, M_0 are the solution of the equation $F(M_0)$=0, which can be solved numerically. We get four roots from Eq. (8).

In Fig. 2, we have shown the variation of $F(M)$ *versus* M for the normalized parameters of the reconnection jet: n_1^0= 0.74, n_2^0=0.26, σ_1= 0.11, σ_2=0.07, U_1=-1.72 and U_2=1.82. It is clear that critical Mach number occurs at the places where the $F(M)$ curve cut the M axis. There are four real roots, R1, R2, R3, and R4 as marked on *Fig. 2*. Critical Mach numbers occurring at R1 and R4 are M_0=2.51 and −2.76, respectively, and they correspond to the fast ion-acoustic modes propagating parallel and anti-parallel to **B**, respectively. It is seen that for $M > |M_0|$, the $F(M)$ curves go below the M-axis, i.e., $F(M)$ <0, thus these are the regular ion-acoustic solitons. The critical Mach numbers associated with R2 and R3 are M_0=1.115 and −0.67, respectively, and they correspond to the slow ion-acoustic modes propagating parallel and anti-parallel to **B**, respectively. In this case, $F(M)$ <0 when $M < |M_0|$. Thus, the slow ion-acoustic solitons belong to the new class of ion-acoustic solitons that can exist below the critical Mach number (Lakhina et al., 2020; Verheest and Hellberg, 2021).

In Figs. 3–6, we have shown the properties of the fast and slow ion-acoustic solitons associated with roots R1 to R4 for the reconnection jet plasma parameters. Sagdeev pseudopotential, $S(\phi, M)$, profiles are obtained from numerical solution of Eq. (7). The profiles of soliton electrostatic potential, ϕ, and electric field, E, are obtained from the numerical solution of Eq. (6).

Fig. 3 shows the properties of fast ion-acoustic solitons (R1) propagating parallel to **B**. From Panel (a) of Fig. 3, it is seen that the fast ion-acoustic solitons have positive potentials. The maximum electrostatic potential ϕ increases with the increase of the Mach number, M, as seen from the curves 1, 2, and 3. For the curve 4, the soliton solution does not exist. Hence there is an upper value for

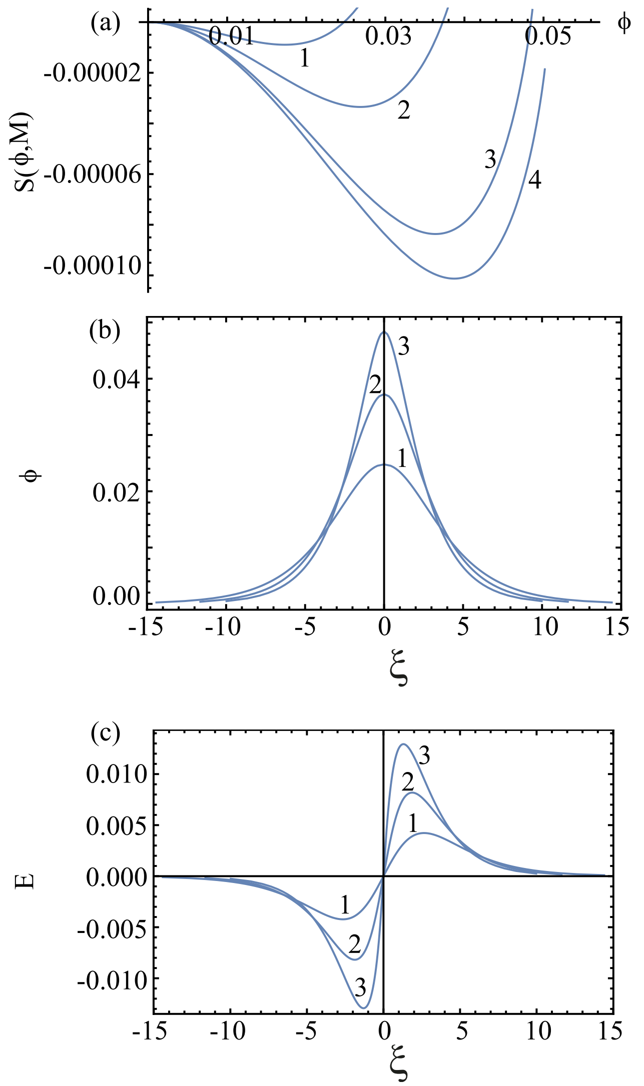

Fig. 3. Properties of fast ion-acoustic solitons (R1) propagating parallel to **B** for the reconnection jet plasma parameters given in Fig. 2. Panel (a) shows variation of Sagdeev pseudopotential $S(\phi, M)$ *versus* the electrostatic potential, ϕ for Mach number M = 2.55, 2.57, 2.59, and 2.595 for the curves 1, 2, 3 and 4, respectively. Curve 4 shows that solitons do not exist for $M \geqslant$2.595. Panel (b) shows soliton electric potential, ϕ, profiles for M = 2.55, 2.57, and 2.59 for the curves 1, 2, and 3, respectively. Panel (c) shows the soliton electric field, E, profiles for M = 2.55, 2.57, and 2.59 for the curves 1, 2, and .3, respectively.

M, say M_{max}, above which soliton solutions do not exist. Panel (b) of Fig. 3, shows the profiles for the potential, ϕ, for the same Mach numbers as those of curve 1, 2 and 3 of Panel (a). It is clear that ϕ profiles have monopolar structures and soliton amplitude increases with increase of M (cf. curves 1, 2 and 3). Panel (c) of Fig. 3 shows that the soliton E profiles have bipolar structures, and their amplitudes increase with increase of M (cf. curves 1, 2 and 3).

Fig. 4 shows the properties of slow ion-acoustic solitons (R2) propagating parallel to **B**. From Panel (a) of Fig. 4, it is seen that the slow ion-acoustic solitons have positive potentials, and the maximum electrostatic potential ϕ

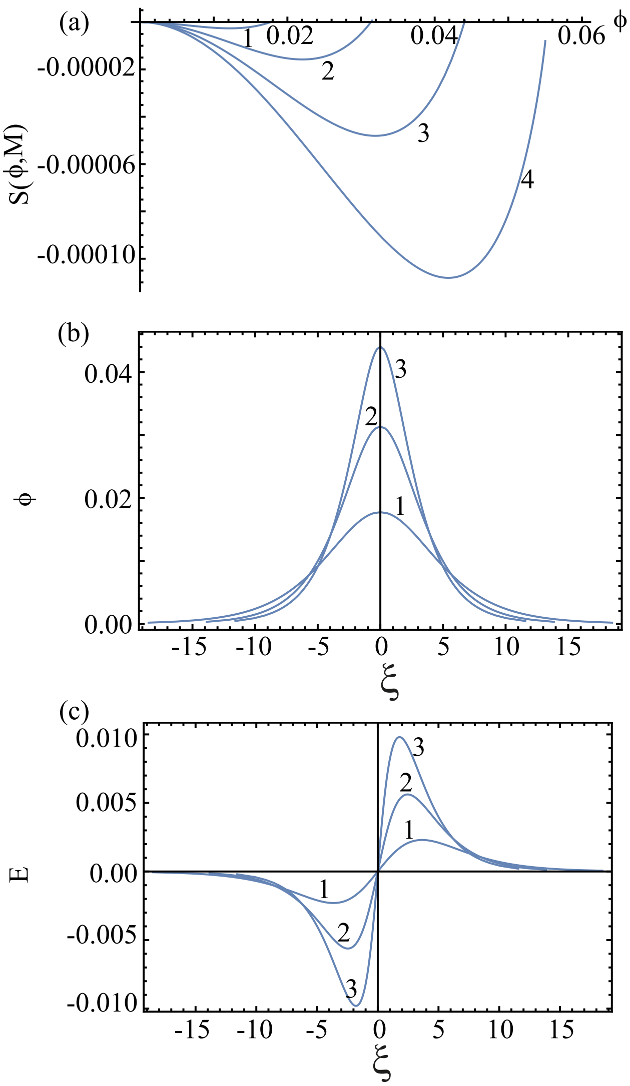

Fig. 4. Properties of slow ion-acoustic solitons (R2) propagating parallel to **B** for the reconnection jet plasma parameters given in Fig. 2. Panel (a) shows variation of Sagdeev pseudopotential $S(\phi, M)$ *versus* the electrostatic potential, ϕ for Mach number M = 1.09, 1.07,1.05 and 1.03 for the curves 1, 2, 3 and 4, respectively. Curve 4 shows that solitons do not exist for $M \leqslant 1.03$. Panel (b) shows soliton ϕ profiles for M = 1.09, 1.07, and 1.05 for the curves 1, 2, and 3, respectively. Panel (c) shows the soliton electric field, E, profiles for M = 1.09, 1.07, and 1.05 for the curves 1, 2, and .3, respectively.

increases with the decrease of the Mach number, M, as seen from the curves 1, 2, and 3. For the curve 4, the soliton solution does not exist. Hence there is a minimum value for M, say M_{min}, below which soliton solutions do not exist. These are the new class of slow ion-acoustic solitons that can exist below the critical Mach number, M_0 (Lakhina et al., 2020). Panel (b) of Fig. 4, it is seen that ϕ profiles have monopolar structures and soliton amplitude increases with a decrease of M (cf. curves 1, 2 and 3). Panel (c) of Fig. 4 shows that the soliton E profiles have bipolar structures, and their amplitudes also increase with a decrease in M (cf. curves 1, 2 and 3).

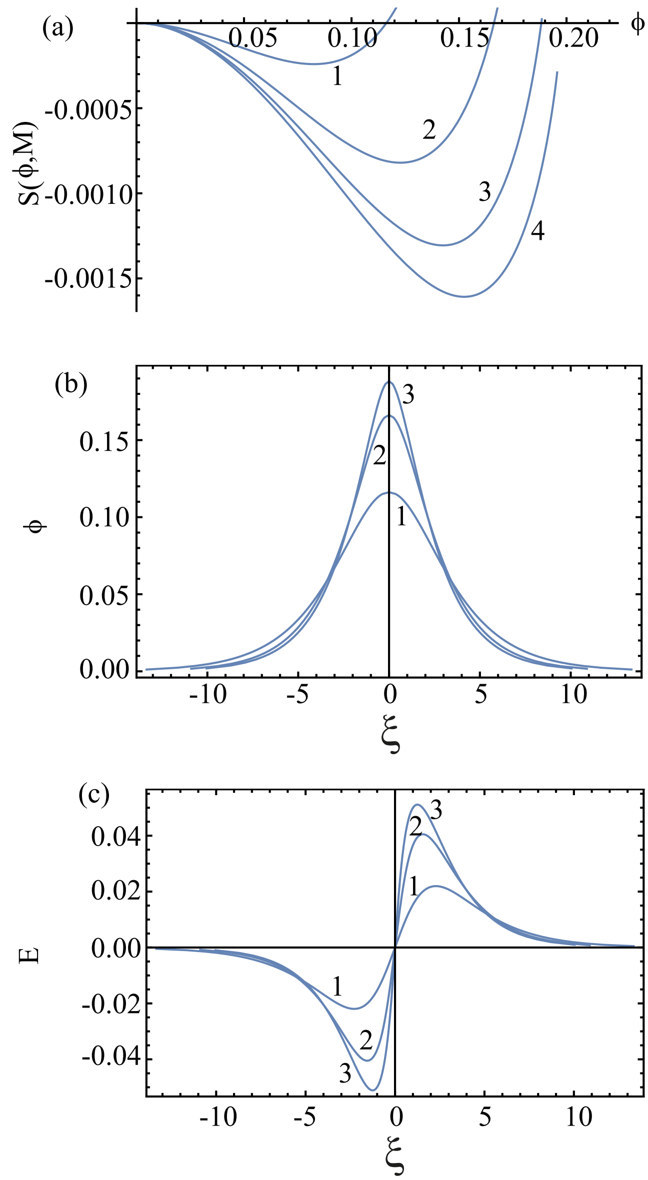

Fig. 5. Properties of slow ion-acoustic solitons (R3) propagating anti-parallel to **B** for the reconnection jet plasma parameters given in Fig. 2. Panel (a) shows variation of Sagdeev pseudopotential $S(\phi, M)$ *versus* the electrostatic potential, ϕ for Mach number $M = -0.59$, -0.55, -0.53, and -0.52 for the curves 1, 2, 3 and 4, respectively. Curve 4 shows that solitons do not exist for $M = -0.52$ or below it. Panel (b) shows soliton ϕ profiles for $M = -0.59$, -0.55, and -0.53 for the curves 1, 2, and 3, respectively. Panel (c) shows the soliton electric field, E, profiles for $M = -0.59$, -0.55, and -0.53 for the curves 1, 2, and .3, respectively.

Fig. 5 shows the properties of slow ion-acoustic solitons (R3) propagating anti-parallel to **B**. From Panel (a) of Fig. 5, it is seen that the slow ion-acoustic solitons have positive potentials, and the maximum electrostatic potential ϕ increases with the decrease of the Mach number, M, as seen from the curves 1, 2, and 3. For the curve 4, the soliton solution does not exist. Hence there is a minimum value for M, say M_{min}, below which soliton solutions do not exist. These are the new class of slow ion-acoustic solitons that can exist below the critical Mach number,

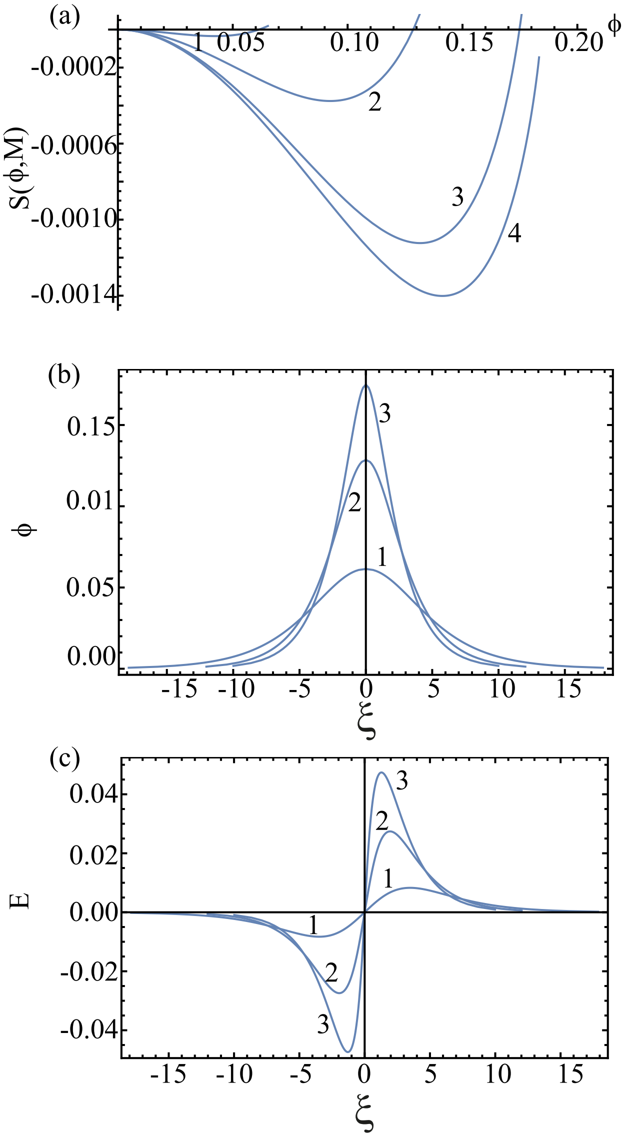

Fig. 6. Properties of fast ion-acoustic solitons (R4) propagating anti-parallel to **B** for the reconnection jet plasma parameters given in Fig. 2. Panel (a) shows variation of Sagdeev pseudopotential $S(\phi, M)$ *versus* the electrostatic potential, ϕ for Mach number M = −2.8, −2.85, −2.89, and −2.9 for the curves 1, 2, 3 and 4, respectively. Curve 4 shows that solitons do not exist for M = −2.9 and above it. Panel (b) shows soliton electric potential, ϕ, profiles for M = −2.8, −2.85, and −2.89 for the curves 1, 2, and 3, respectively. Panel (c) shows the soliton electric field, E, profiles for M = −2.8, −2.85, −2.89 for the curves 1, 2, and .3, respectively.

M_0 (Lakhina et al., 2020). Panel (b) of Fig. 5 shows that ϕ profiles have monopolar structures, and their amplitudes increase with a decrease of M (cf. curves 1, 2 and 3). Panel (c) of Fig. 4 shows bipolar profiles of the soliton E field. The amplitudes of E increase with a decrease in M (cf. curves 1, 2 and 3).

Fig. 6 shows the properties of fast ion-acoustic solitons (R4) propagating anti-parallel to **B**. Panel (a) of Fig. 6 shows that the fast ion-acoustic solitons have positive potentials. The maximum electrostatic potential ϕ increases with the increase of the Mach number, M, as seen from the curves 1, 2, and 3. The soliton solution does not exist for M=M_{max}=-2.9 (cf curve 4). Panel (b) of Fig. 6, it is clear that ϕ profiles have monopolar structures, and soliton amplitude increases with an increase of M (cf. curves 1, 2 and 3). Panel (c) of Fig. 6 shows that the soliton E profiles have bipolar structures, and their amplitudes increase with increase of M (cf. curves 1, 2 and 3).

The properties of the ion-acoustic solitons, associated with roots R1 to R4, in terms of unnormalized quantities, such as their velocities, V, width, W, electric field, E, and electric potential, ϕ, are listed in Tables 1. Here the soliton width, W, is defined as the full width at half maximum. Columns 1 and 2 describe the root and the mode associated with it, respectively. Column 3 gives the Mach number associated with curves 1, 2 and 3 of the respective figure, Columns 4–7 show the soliton velocity, V in km s^{-1}, width W in km, electric field, E in mV m^{-1} and electric potential, ϕ in volts, respectively. From Table 1, Rows 1 and 4, it is clear that for fast ion-acoustic solitons (R1 and R4), the soliton speeds, V, electric fields, E, potential, ϕ, are increased and widths W are decreased with increasing Mach numbers. On the other hand, from Table 1 and Rows 2 and 3, it is seen that for slow ion-acoustic solitons (R2 and R3), speeds, V, and widths W increase but the magnitudes of E and ϕ decrease with increasing Mach numbers.

4. Comparison with reconnection jet ESWs

For the parameters of reconnection jet plasma, we get the ion-acoustic speed, C_a=523 km s^{-1}, and Debye length, λ_{De}= 2.12 km. From Table 1, we see that all fast and slow ion-acoustic solitons have positive potentials and the electric fields are in the range of E=(3–68) mV m^{-1}, which are in agreement with the polarity and the electric fields of ESWs observed in the reconnection jet. The fast ion-acoustic solitons (R1) and slow ion-acoustic solitons (R2) propagate parallel to **B**. The fast ion-acoustic (R1) solitons have velocities, electric fields, potentials and widths in range of (1334–1355) km s^{-1}, (5–17) mV m^{-1}, (70–138) V, and (9–16) km, respectively. The slow ion-acoustic (R2) solitons have V, E, ϕ and W in the range of (550–570) km s^{-1}, (3–13) mV m^{-1}, (50–125) V, and (12–22) km, respectively. The electric fields, potentials and widths of both fast (R1) and slow (R2) ion-acoustic solitons match with the observed values of ESWs. While the velocities of slow ion-acoustic (R2) solitons are in good agreement with those of the ESWs, the velocities of the fast ion-acoustic (R1) are on the higher side. However, both slow (R2) and fast (R1) propagates parallel to the magnetic field while the ESWs are observed to propagate anti-parallel to **B**.

From Table 1, we notice that the slow ion-acoustic solitons (R3) and fast ion-acoustic solitons (R4) propagate anti-parallel to **B**, in agreement with the propagation direction of observed ESWs in the reconnection jet. The slow ion-acoustic (R3) solitons have velocities, electric fields,

Table 1
Properties of ion-acoustic solitons corresponding to the reconnection jet parameters (Liu et al., 2019): density of proton beam 1, $N_1 = 0.026\ \text{cm}^{-3}$, temperature of proton beam 1, $T_1 = 300$ eV, streaming speed of proton beam 1, $V_1 = -900\ \text{km s}^{-1}$, density of proton beam 2, $N_2 = 0.009\ \text{cm}^{-3}$, temperature of proton beam 2, $T_2 = 200$ eV, streaming speed of proton beam 2, $V_2 = 950\ \text{km s}^{-1}$, electron density, $N_e = 0.035\ \text{cm}^{-3}$, and electron temperature, $T_e = 2.86$ keV. Then, the ion-acoustic speed is $C_a = 523\ \text{km s}^{-1}$, and Debye length is $\lambda_{De} = 2.12$ km. Here, V is the phase velocity, W is the width, E is the electric field, and ϕ is the electrostatic potential of the solitons

Roots	Mode	Mach Number	V (km/s)	W (km)	E (mV/m)	ϕ (V)
R1	Fast ion-acoustic parallel to **B**	2.55	1334.47	16.412	5.7	70.91
		2.57	1344.93	12.455	11	106.60
		2.59	1355.4	9.808	17.4	138.48
R2	Slow ion-acoustic parallel to **B**	1.09	570	21.829	3.1	50.73
		1.07	559.95	15.515	7.6	89.66
		1.05	549.49	12.171	13.2	125.99
R3	Slow ion-acoustic anti-parallel to **B**	−0.59	−308.76	14.662	29.6	332.46
		−0.55	−287.83	11.048	54.5	475.64
		−0.53	−277.36	9.646	68.8	538.63
R4	Fast ion-acoustic anti-parallel to **B**	−2.8	−1465.3	20.943	11.2	175.69
		−2.85	−1491.46	12.867	36.92	367.81
		−2.89	−1512.4	9.714	63.82	500.11

potentials and widths in the range of (−277 to −304) km s^{-1}, (29–68) mV m^{-1}, (330–540) V, and (9–15) km, respectively. The fast ion-acoustic (R4) solitons have V, E, ϕ and W in the range of (−1465 to −1512) km s^{-1}, (11–64) mV m^{-1}, (175–500) V, and (9–21) km, respectively.

The electric fields and width for both fast (R4) and slow (R3) ion-acoustic solitons more or less match with the observed values of ESWs, but the speeds are higher for the former, and slower for the latter solitons than the observed speed. The electric potentials of the fast (R4) ion-acoustic solitons contain the observed potential of ESWs, but the potentials of the slow (R3) ion-acoustic solitons are on the higher side of the observed potentials.

5. Summary and discussion

Recently, Lakhina et al. (2020) have developed an ion-acoustic soliton model based on fluid equations for a plasma system consisting of hot Maxwellian electrons, and two counterstreaming ion beams, a situation similar to the reconnection jet plasma. We use this model to explain the ESWs observed in the reconnection jet region of the Earth's magnetotail (Liu et al., 2019). When the observed parameters of the reconnection jet plasma are taken as the input for the theoretical model, it predicts four types of ion-acoustic solitons, namely, two fast ion-acoustic (R1 and R4) solitons, and two slow ion-acoustic (R2 and R3) solitons. The solutions R1 to R4 represent the nonlinear eigenmodes of the system. The fast (R1) and slow (R2) ion-acoustic solitons propagate parallel to the magnetic field, **B**, whereas the other fast (R4) and slow (R3) ion-acoustic solitons propagate anti-parallel to **B**. The slow ion-acoustic solitons (R2 and R3) belongs to the new class of ion-acoustic solitons that can exist below the critical Mach number.

The observed properties of reconnection jet ESWs as reported by Liu et al. (2019) are: bipolar electric fields, $E \sim$ (5–30) mV m^{-1}, positive potentials $\phi \sim$ (50–200) V, velocity anti-parallel to $\mathbf{B} = -\ 820 \times 0.79 \approx -\ 650\ \text{km s}^{-1}$, widths, $W = 9.5\ \lambda_{De} = 20$ km. From Table 1 and Figs. 3–6, one can see that all (R1 to R4) ion-acoustic solitons have bipolar electric fields in the range of $E \sim$ (3–68) mV m^{-1}, and widths $W \sim$ (9–22) km, which are in good agreement with the observations. The potentials associated with fast (R1) and slow (R2) ion-acoustic solitons are in the range of $\phi \sim$ (50–138) V, which is again in good agreement with the observed ESWs potentials. However, both fast (R1) and slow (R2) ion-acoustic solitons propagate parallel to **B** with speeds in the range of ∼ (1334–1355) km s^{-1} and ∼ (550–570) km s^{-1}, respectively. This does not agree with the propagation direction of ESWs being anti-parallel to **B**, though the speed of slow (R2) ion-acoustic soliton seems to be in fair agreement with the magnitude of ESWs speed.

The potentials associated with fast (R4) and slow (R3) ion-acoustic solitons are in the range of $\phi \sim$ (175–538) V, which are on the higher side of the observed ESWs potentials. However, both fast (R4) and slow (R3) ion-acoustic solitons propagate anti-parallel to **B** with speeds in the range of ∼ (−1465 to −1512) km s^{-1} and ∼ (−277 to −308) km s^{-1}, respectively. This does agree with the anti-parallel to **B** propagation direction of observed ESWs, though the speeds of fast (R4) ion-acoustic solitons are higher and that of the slow (R3) ion-acoustic solitons are smaller by a factor of 2 than the observed ESWs speeds. We can speculate several reasons for the speed mismatch. Firstly, the speed mismatch can result from uncertainty in the method used by Liu et al. (2019), to obtain the observed wave speed. In their observations, the waveforms captured by different satellites are not exactly the same, possibly leading to some uncertainty in the timing result. Secondly, the ion beams observed during the ESW wave period might not be the original beam which generated the waves. Thirdly, the speed mismatch may be due to the missing ion species, for example due to either missing oxygen ion beams as discussed by Liu et al. (2019) while doing the linear stability analysis or the missing background protons. Including either the oxygen ions or background protons in the system would yield 6 solutions, R1 to R4 (as discussed here, but with different Mach number values) and two new solutions R5 and R6. Liu et al. (2019) found that introducing oxygen ions gives better match between the phase speed of the excited mode and the observed ESW speed. We speculate that one or more of the new solutions R1 to R6 would have Mach number closer to the observed ESW speed.

We would like to point out that though Liu et al. (2019) did not observe ESWs propagating parallel to **B**, as predicted by our model, it does not mean that parallel propagating ESWs do not exist in the reconnection jet. A possible explanation would be that all MMS spacecraft were behind the generation region of ESWs in the reconnection jet, and could therefore record only the ESWs propagating anti-parallel to the magnetic field. To sum up, the ion-acoustic soliton model provides a plausible explanation for the occurrence of parallel propagating ESWs in the reconnection jet. As the model is general, we speculate that ion-acoustic solitons could exist in reconnection jets of astrophysical plasmas, even though *in situ* measurements of particle distribution functions and electric field are not available.

Data Availability

The data used in the manuscript is taken from Liu et al., Ion-beam driven intense electrostatic solitary waves in reconnection jet, Geophys. Res. Lett., 46 [2019]. https://doi.org/10.1029/2019GL085419.

Declaration of Competing Interest

The authors declare that they have no known competing financial interests or personal relationships that could have appeared to influence the work reported in this paper.

Acknowledgements

GSL thanks the Indian National Science Academy (INSA), New Delhi for the support under the INSA Honorary Scientist Scheme.

References

Angelopoulos, V., Baumjohann, W., Kennel, C.F., Coroniti, F.V., Kivelson, M.G., Pellat, R., et al., 1992. Bursty bulk flows in the inner central plasma sheet. J. Geophys. Res. 97, 4027–4039. https://doi.org/10.1029/91JA02701.

Angelopoulos, V., McFadden, J., Larson, D., Carlson, C.W., Mende, S. B., Frey, H., et al., 2008. Tail reconnection triggering substorm onset. Science 321, 931–935. https://doi.org/10.1126/science.1160495.

Bale, S.D., Kellogg, P.J., Larsen, D.E., Lin, R.P., Goetz, K., Lepping, R. P., 1998. Bipolar electrostatic structures in the shock transition region: Evidence of electron phase space holes. Geophys. Res. Lett. 25, 2929–2932. https://doi.org/10.1029/98GL02111.

Bernstein, I.B., Greene, J.M., Kruskal, M.D., 1957. Exact nonlinear plasma oscillations. Phys. Rev. 108, 546–550. https://doi.org/10.1103/PhysRev.108.546.

Berthomier, M., Pottelette, R., Malingre, M., 1998. Solitary waves and weak double layers in a two-electron temperature auroral plasma. J. Geophys. Res. 103, 4261–4270. https://doi.org/10.1029/97JA00338.

Berthomier, M., Pottelette, R., Malingre, M., Khotyaintsev, Y., 2000. Electron-acoustic solitons in an electron-beam plasma system. Phys. Plasmas 7, 2987–2994. https://doi.org/10.1063/1.874150.

Birn, J., Hesse, M., 2014. Forced reconnection in the near magnetotail: Onset and energy conversion in pic and mhd simulations. J. Geophys. Res.: Space Physics 119, 290–309. https://doi.org/10.1002/2013JA019354.

Boström, R., Gustafsson, G., Holback, B., Holmgren, G., Koskinen, H., Kintner, P., 1988. Characteristics of solitary waves and weak double layers in the magnetospheric plasma. Phys. Rev. Lett. 61, 82–85. https://doi.org/10.1103/PhysRevLett.61.82.

Bounds, S.R., Pfaff, R.F., Knowlton, S.F., Mozer, F.S., Temerin, M.A., Kletzing, C.A., 1999. Solitary potential structures associated with ion and electron beams near 1re altitude. J. of Geophys. Res. 104, 28709–28717. https://doi.org/10.1029/1999JA900284.

Cao, J., Ma, Y., Parks, G., Reme, H., Dandouras, I., Zhang, T., 2013. Kinetic analysis of the energy transport of bursty bulk flows in the plasma sheet. J. Geophys. Res. 118, 313–320. https://doi.org/10.1029/2012JA018351.

Cao, J.B., Ma, Y.D., Parks, G., Reme, H., Dandouras, I., Nakamura, R., et al., 2006. Joint observations by cluster satellites of bursty bulk flows in the magnetotail. J. Geophys. Res. 111, A04206. https://doi.org/10.1029/2005JA011322.

Cattaert, T., Verheest, F., Hellberg, M., 2005. Potential hill electron-acoustic solitons and double layers in plasmas with two electron species. Phys. Plasmas 12, 042901. https://doi.org/10.1063/1.1868733.

Cattell, C.A., Dombeck, J., Wygant, J.R., Hudson, M.K., Mozer, F.S., Temerin, M.A., Peterson, W.K., Kletzing, C.A., Russell, C.T., Pfaff, R.F., 1999. Comparisons of polar satellite observations of solitary wave velocities in the plasma sheet boundary and the high altitude cusp to those in the auroral zone. Geophys. Res. Lett. 26, 425–428. https://doi.org/10.1029/1998GL900304.

Che, H., Drake, J.F., Swisdak, M., Yoon, P.H., 2010. Electron holes and heating in the reconnection dissipation region. Geophys, Res. Lett. 37, L11105. https://doi.org/10.1029/2010GL043608.

Chen, G., Fu, H.S., Zhang, Y., Li, X., Ge, Y.S., Du, A.M., et al., 2019. Energetic electron acceleration in unconfined reconnection jets. Astrophys. J. Lett. 881, L8. https://doi.org/10.3847/2041-8213/ab3041.

Chen, L.-J., Pickett, J., Kintner, P., Franz, J., Gurnett, D., 2005. On the width-amplitude inequality of electron phase space holes. J. Geophys. Res. 110. https://doi.org/10.1029/2005JA011087.

Deng, X., Ashour-Abdalla, M., Zhou, M., Walker, R., El-Alaoui, M., Angelopoulos, V., et al., 2010. Energy range of electron rolling-pin distribution behind dipolarization front. J. Geophys. Res. 115, A09225. https://doi.org/10.1029/2009JA015107.

Divin, A., Khotyaintsev, Y.V., Vaivads, A., André, M., 2017. Lower hybrid drift instability at a dipolarization front. Journal of Geophysical Research: Space Physics 120, 1124–1132. https://doi.org/10.1002/2014JA020528.

Drake, J.F., Swisdak, M., Cattell, C., Shay, M.A., Rogers, B.N., Zeiler, A., 2003. Formation of electron holes and particle energization during magnetic reconnection. Science 5608, 873–877. https://doi.org/10.1126/science.1080333.

Drenkhahn, G., Spruit, H.C., 2002. Efficient acceleration and radiation in poynting flux powered grb outflows. A&A 391, 1141–1153. https://doi.org/10.1051/0004-6361:20020839.

Dubouloz, N., Pottelette, R., Malingre, M., Treumann, R.A., 1991. Generation of broadband electrostatic noise by electron acoustic

solitons. Geophys. Res. Lett. 18, 155–158. https://doi.org/10.1029/90GL02677.
Dubouloz, N., Treumann, R.A., Pottelette, R., Malingre, M., 1993. Turbulence generated by a gas of electron acoustic solitons. J. Geophys. Res. 98, 17415–17422. https://doi.org/10.1029/93JA01611.
Dungey, J.W., 1961. Interplanetary magnetic field and the auroral zones. Phys. Res. Lett. 6, 47–48. https://doi.org/10.1103/PhysRevLett.6.47.
Ergun, R.E., Carlson, C.W., McFadden, J.P., Mozer, F.S., Delory, G.T., Peria, W., Chaston, C.C., Temerin, M., Roth, I., Muschietti, L., Elphic, R., Strangeway, R., Pfaff, R., Cattell, C.A., Klumpar, D., Shelley, E., Peterson, W., Moebius, E., Kistler, L., 1998a. Fast satellite observations of large-amplitude solitary structures. Geophys. Res. Lett. 25, 2041–2044. https://doi.org/10.1029/98GL00636.
Ergun, R.E., Carlson, C.W., McFadden, J.P., Mozer, F.S., Muschietti, L., Roth, I., Strangeway, R.J., 1998b. Debye-scale plasma structures associated with magnetic-field-aligned electric fields. Phys. Rev. Lett. 81, 826–829. https://doi.org/10.1103/PhysRevLett.81.826, URL: https://link.aps.org/doi/10.1103/PhysRevLett.81.826.
Ergun, R.E., Goodrich, K.A., Stawarz, J.E., Andersson, L., Angelopoulos, V., 2014. Large-amplitude electric fields associated with bursty bulk flow braking in the earth's plasma sheet. Journal of Geophysical Research: Space Physics 120, 1832–1844. https://doi.org/10.1002/2014JA020165.
Franz, J.R., Kintner, P.M., Pickett, J.S., 1998. Polar observations of coherent electric field structures. Geophys. Res. Lett. 25, 1277–1280. https://doi.org/10.1029/98GL50870.
Franz, J.R., Kintner, P.M., Pickett, J.S., Chen, L.-J., 2005. Properties of small-amplitude electron phase-space holes observed by polar. J. Geophys. Res. 110. https://doi.org/10.1029/2005JA011095.
Fu, H.S., Cao, J.B., Cully, C.M., Khotyaintsev, Y.V., Vaivads, A., Angelopoulos, V., et al., 2014. Whistler-mode waves inside flux pileup region: Structured or unstructured? Journal of Geophysical Research: Space Physics 119, 9089–9100. https://doi.org/10.1002/2014JA020204.
Fu, H.S., Khotyaintsev, Y.V., André, M., Vaivads, A., 2011. Fermi and betatron acceleration of suprathermal electrons behind dipolarization fronts. Geophys. Res. Lett. 38, L16104. https://doi.org/10.1029/2011GL048528.
Fu, H.S., Vaivads, A., Khotyaintsev, Y.V., André, M., Cao, J.B., Olshevsky, V., et al., 2017. Intermittent energy dissipation by turbulent reconnection. Geophys. Res. Lett. 44, 37–43. https://doi.org/10.1002/2016GL071787.
Ghosh, S.S., Pickett, J.S., Lakhina, G.S., Winningham, J.D., Lavraud, B., Décréau, P.M.E., 2008. Parametric analysis of positive amplitude electron acoustic solitary waves in a magnetized plasma and its application to boundary layers. J. Geophys. Res. 113. https://doi.org/10.1029/2007JA012768.
Giovanelli, R.G., 1947. Magnetic and electric phenomena in the sun's atmosphere associated with sunspots. Month. Not. Roy. Astron. Soc. 107, 338–355. https://doi.org/10.1093/mnras/107.4.338.
Goldman, M.V., Oppenheim, M.M., Newman, D.L., 1999. Nonlinear two-stream instabilities as an explanation for auroral bipolar wave structures. Geophys. Res. Lett. 26, 1821–1824. https://doi.org/10.1029/1999GL900435.
Graham, D.B., Khotyaintsev, Y.V., Vaivads, A., André, M., 2015. Electrostatic solitary waves with distinct speeds associated with asymmetric reconnection. Geophys. Res. Lett. 42, 215–224. https://doi.org/10.1002/2014GL062538.
Huang, C., Lu, Q., Wang, P., Wu, M., Wang, S., 2014. Characteristics of electron holes generated in the separatrix region during antiparallel magnetic reconnection. Journal of Geophysical Research: Space Physics 119, 6445–6454. https://doi.org/10.1002/2014JA019991.
Huang, S.Y., Zhou, M., Deng, X.H., Yuan, Z.G., Pang, Y., Wei, Q., et al., 2012. Kinetic structure and wave properties associated with sharp dipolarization front observed by cluster. Annales de Geophysique 30, 97–107. https://doi.org/10.5194/angeo-30-97-2012.
Hudson, M.K., Lotko, W., Roth, I., Witt, E., 1983. Solitary waves and double layers on auroral field lines. J. Geophys. Res. 88, 916–926. https://doi.org/10.1029/JA088iA02p00916.
Hutchinson, I.H., 2017. Electron holes in phase space: What they are and why they matter. Phys. Plasmas 24, 055601. https://doi.org/10.1063/1.4976854.
Hwang, K.-J., Goldstein, M.L., Vinas, A.F., Schriver, D., Ashour-Abdalla, M., 2014. Wave-particle interactions during a dipolarization front event. Journal of Geophysical Research: Space Physics 119, 2484–2493. https://doi.org/10.1002/2013JA019259.
Jovanović, D., Shukla, P.K., 2000. Nonlinear model for coherent electric field structures in the magnetosphere. Phys. Rev. Lett. 84, 4373–4376. https://doi.org/10.1103/PhysRevLett.84.4373.
Kakad, A., Kakad, B., Anekallu, C., Lakhina, G., Omura, Y., Fazakerley, A., 2016. Slow electrostatic solitary waves in earth's plasma sheet boundary layer. J. Geophys. Res. 121, 4452–4465. https://doi.org/10.1002/2016JA022365.
Kakad, A.P., Singh, S.V., Reddy, R.V., Lakhina, G.S., Tagare, S.G., Verheest, F., 2007. Generation mechanism for electron acoustic solitary waves. Phys. Plasmas 14, 052305. https://doi.org/10.1063/1.2732176.
Khotyaintsev, Y.V., Cully, C.M., Vaivads, A., André, M., Owen, C.J., 2011. Plasma jet braking: Energy dissipation and nonadiabatic electrons. Phys. Rev. Lett. 106, 16. https://doi.org/10.1103/PhysRevLett.106.165001.
Khotyaintsev, Y.V., Vaivads, A., André, M., Fujimoto, M., Retino, A., Owen, C.J., 2010. Observations of slow electron holes at a magnetic reconnection site. Phys. Rev. Lett. 105, 165002. https://doi.org/10.1103/PhysRevLett.105.165002.
Kirk, J.G., Skjaeraasen, O., 2003. Dissipation in poynting-flux-dominated flows: The σ-problem of the crab pulsar wind. ApJ 591, 366–379. https://doi.org/10.1086/375215.
Kojima, H., Matsumoto, H., Chikuba, S., Horiyama, S., Ashour-Abdalla, M., Anderson, R.R., 1997. Geotail waveform observations of broadband/narrowband electrostatic noise in the distant tail. J. of Geophys. Res. 102, 14439–14455. https://doi.org/10.1029/97JA00684.
Koskinen, H.E.J., Lundin, R., Holback, B., 1990. On the plasma environment of solitary waves and weak double layers. J. Geophys. Res. 95, 5921–5929. https://doi.org/10.1029/JA095iA05p05921.
Lakhina, G.S., 2000. Magnetic reconnection. Bull. Astron. Soc. India 28, 593–646.
Lakhina, G.S., Kakad, A.P., Singh, S.V., Verheest, F., 2008a. Ion- and electron-acoustic solitons in two-electron temperature space plasmas. Phys. Plasmas 15, 062903. https://doi.org/10.1063/1.2930469.
Lakhina, G.S., Singh, S.V., Kakad, A.P., 2014. Ion acoustic solitons/double layers in two - ion plasma. Phys. Plasmas 21, 062311. https://doi.org/10.1063/1.4884791.
Lakhina, G.S., Singh, S.V., Kakad, A.P., Goldstein, M.L., Viñas, A.F., Pickett, J.S., 2009. A mechanism for electrostatic solitary structures in the earth's magnetosheath. J. Geophys. Res. 114. https://doi.org/10.1029/2009JA014306.
Lakhina, G.S., Singh, S.V., Kakad, A.P., Pickett, J.S., 2011. Generation of electrostatic solitary waves in the plasma sheet boundary layer. J. Geophys. Res. 116. https://doi.org/10.1029/2011JA016700.
Lakhina, G.S., Singh, S.V., Kakad, A.P., Verheest, F., Bharuthram, R., 2008b. Study of nonlinear ion- and electron-acoustic waves in multi-component space plasmas. Nonlinear Processes in Geophysics 15, 903–913. https://doi.org/10.5194/npg-15-903-2008.
Lakhina, G.S., Singh, S.V., Rubia, R., 2020. A new class of ion-acoustic solitons that can exist below critical mach number. Phys. Scr. 95, 105601. https://doi.org/10.1088/1402-4896/abb2e0.
Lakhina, G.S., Singh, S.V., Rubia, R., Sreeraj, T., 2018. A review of nonlinear fluid models for ion-and electron-acoustic solitons and double layers: Application to weak double layers and electrostatic solitary waves in the solar wind and the lunar wake. Phys. Plasmas 25, 080501. https://doi.org/10.1063/1.5033498.
Lapenta, G., Goldman, M., Newman, D., Markidis, S., Divin, A., 2014. Electromagnetic energy conversion in downstream fronts from three dimensional kinetic reconnection. Phys. Plasmas 21, 5. https://doi.org/10.1063/1.4872028.
Larrabee, D.A., Lovelace, R.V.E., Romanova, M.M., 2003. Efficient acceleration and radiation in poynting flux powered grb outflows. ApJ 586, 72–78. https://doi.org/10.1086/367640.

Liu, C.M., Fu, H.S., Vaivads, A., Khotyaintsev, Y.V., Gershman, D.J., Hwang, K.J., et al., 2018a. Electron jet detected by mms at dipolarization front. Geophys. Res. Lett. 45, 556–564. https://doi.org/10.1002/2017GL076509.

Liu, C.M., Fu, H.S., Xu, Y., Cao, J.B., Liu, W.L., 2017. Explaining the rolling-pin distribution of suprathermal electrons behind dipolarization fronts. Geophys. Res. Lett. 44, 6492–6499. https://doi.org/10.1002/2017GL074029.

Liu, C.M., Fu, H.S., Xu, Y., Khotyaintsev, Y.V., Burch, J.L., Ergun, R. E., et al., 2018b. Electron-scale measurements of dipolarization front. Geophys. Res. Lett. 45, 4628–4638. https://doi.org/10.1029/2018GL077928.

Liu, C.M., Vaivads, A., Graham, D.B., Khotyaintsev, Y.V., Fu, H.S., Johlander, A., André, M., Giles, B.L., 2019. Ion-beam-driven intense electrostatic solitary waves in reconnection jet. Geophys. Res. Lett. 46, 1–9. https://doi.org/10.1029/2019GL085419.

Lu, S., Angelopoulos, V., Fu, H.S., 2016. Suprathermal particle energization in dipolarization fronts: Particle-in-cell simulations. J. Geophys. Res.: Space Physics 121, 9483–9500. https://doi.org/10.1002/2016JA022815.

Maharaj, S., Bharuthram, R., Singh, S.V., Lakhina, G.S., 2015. Existence domains of slow and fast ion-acoustic solitons in two-ion space plasmas. Phys. Plasmas 22, 032313. https://doi.org/10.1063/1.4916319.

Maharaj, S.K., Bharuthram, R., Singh, S., Lakhina, G., 2012a. Existence domains of arbitrary amplitude nonlinear structures in two-electron temperature space plasmas. ii. high-frequency electron-acoustic solitons. Phys. Plasmas 19, 122301. https://doi.org/10.1063/1.4769174.

Maharaj, S.K., Bharuthram, R., Singh, S.V., Lakhina, G.S., 2012b. Existence domains of arbitrary amplitude nonlinear structures in two-electron temperature space plasmas. i. low-frequency ion-acoustic solitons. Phys. Plasmas 19, 072320. https://doi.org/10.1063/1.4737895.

Mahmood, S., Ur-Rehman, H., 2013. Compressive and rarefactive for fast and slow ion-acoustic waves in multi-ion plasmas. J. Phys. Soc. Japan 82, 074501. https://doi.org/10.7566/JPSJ.82.074501.

Matsumoto, H., Kojima, H., Miyatake, T., Omura, Y., Okada, M., Nagano, I., Tsutsui, M., 1994. Electrostatic solitary waves (esw) in the magnetotail: Ben wave forms observed by geotail. Geophys. Res. Lett. 21, 2915–2918. https://doi.org/10.1029/94GL01284.

Mozer, F.S., Agapitov, O.V., Artemyev, A., Drake, J.F., Krasnoselskikh, V., Lejosne, S., Vasko, I., 2015. Time domain structures: What and where they are, what they do, and how they are made. Geophys. Res. Lett. 42, 3627–3638. https://doi.org/10.1002/2015GL063946.

Muschietti, L., Ergun, R.E., Roth, I., Carlson, C.W., 1999. Phase-space electron holes along magnetic field lines. Geophys. Res. Lett. 26, 1093–1096. https://doi.org/10.1029/1999GL900207.

Norgren, C., Andre, M., Vaivads, A., Khotyaintsev, Y.V., 2015. Slow electron phase space holes: Magnetotail observations. Geophys. Res. Lett. 42, 1654–1661. https://doi.org/10.1002/2015GL063218.

Omura, Y., Kojima, H., Miki, N., Mukai, T., Matsumoto, H., Anderson, R., 1999. Electrostatic solitary waves carried by diffused electron beams observed by the geotail spacecraft. J. Geophys. Res. 104, 14627–14637. https://doi.org/10.1029/1999JA900103.

Omura, Y., Matsumoto, H., Miyake, T., Kojima, H., 1996. Electron beam instabilities as generation mechanism of electrostatic solitary waves in the magnetotail. J. Geophys. Res. 101, 2685–2697. https://doi.org/10.1029/95JA03145.

Pan, D.-X., Khotyaintsev, Y.V., Graham, D.B., Vaivads, A., Zhou, X.-Z., André, M., et al., 2018. Rippled electron-scale structure of a dipolarization front. Geophys. Res. Lett. 45, 12116–12124. https://doi.org/10.1029/2018GL080826.

Pickett, J.S., Chen, L.-J., Kahler, S.W., Santolík, O., Goldstein, M.L., Lavraud, B., Décréau, P.M.E., Kessel, R., Lucek, E., Lakhina, G.S., Tsurutani, B.T., Gurnett, D.A., Cornilleau-Wehrlin, N., Fazakerley, A., Rème, H., Balogh, A., 2005. On the generation of solitary waves observed by cluster in the near-earth magnetosheath. Nonlinear Proc. Geoph. 12, 181–193. https://doi.org/10.5194/npg-12-181-2005.

Pickett, J.S., Chen, L.-J., Kahler, S.W., Santolík, O., Gurnett, D.A., Tsurutani, B.T., Balogh, A., 2004. Isolated electrostatic structures observed throughout the cluster orbit: relationship to magnetic field strength. Ann. Geophys. 22, 2515–2523. https://doi.org/10.5194/angeo-22-2515-2004.

Pickett, J.S., Menietti, J.D., Gurnett, D.A., Tsurutani, B., Kintner, P.M., Klatt, E., Balogh, A., 2003. Solitary potential structures observed in the magnetosheath by the Cluster spacecraft. Nonlin. Process. Geophys. 10, 3–11.

Pottelette, R., Ergun, R.E., Treumann, R.A., Berthomier, M., Carlson, C.W., McFadden, J.P., Roth, I., 1999. Modulated electron-acoustic waves in auroral density cavities: Fast observations. Geophys. Res. Lett. 26, 2629–2632. https://doi.org/10.1029/1999GL900462.

Pottelette, R., Malingre, M., Dubouloz, N., Aparicio, B., Lundin, R., Holmgren, G., Marklund, G., 1990. High-frequency waves in the cusp/cleft regions. J. Geophys. Res. 95, 5957–5971. https://doi.org/10.1029/JA095iA05p05957.

Reddy, R.V., Lakhina, G., Verheest, F., 1992. Ion-acoustic double layers and solitons in multispecies auroral beam-plasmas. Planet. Space Sci. 40, 1055–1062. https://doi.org/10.1016/0032-0633(92)90034-L.

Reddy, R.V., Lakhina, G.S., 1991. Ion acoustic double layers and solitons in auroral plasma. Planet. Space Sci. 39, 1343–1350. https://doi.org/10.1016/0032-0633(91)90015-3.

Rubia, R., Singh, S.V., Lakhina, G.S., 2016. Existence domains of electrostatic solitary structures in the solar wind plasma. Phys. Plasmas 23, 062902. https://doi.org/10.1063/1.4953892.

Rubia, R., Singh, S.V., Lakhina, G.S., 2017. Occurrence of electrostatic solitary waves in the lunar wake. J. Geophys. Res. 122, 9134–9147. https://doi.org/10.1002/2017JA023972.

Rubia, R., Singh, S.V., Lakhina, G.S., 2018. Existence domain of electrostatic solitary waves in the lunar wake. Phys. Plasmas 25, 032302. https://doi.org/10.1063/1.5017638.

Rufai, O.R., Bharuthram, R., Singh, S.V., Lakhina, G.S., 2015. Effect of excess superthermal hot electrons on finite amplitude ion-acoustic solitons and supersolitons in a magnetized auroral plasma. Phys. Plasmas 22, 102305. https://doi.org/10.1063/1.4933000.

Schamel, H., 1982. Kinetic theory of phase space vortices and double layers. Phys. Scripta 1982, 228, URL: http://stacks.iop.org/1402-4896/1982/i=T2A/a=030.

Shibata, K., Masuda, S., Shimojo, M., Hara, H., Yokoyama, T., Tsuneta, S., Kosugi, T., Ogawara, Y., 1995. Hot-plasma ejections associated with compact-loop solar flares. ApJ 451, L83–L85. https://doi.org/10.1086/309688.

Singh, N., Khazanov, G., 2003. Double layers in expanding plasmas and their relevance to the auroral plasma processes. J. Geophys. Res. 108. https://doi.org/10.1029/2002JA009436.

Singh, N., Loo, S.M., Wells, E., 2001a. Electron hole structure and its stability depending on plasma magnetization. J. Geophys. Res. 106, 21183–21198. https://doi.org/10.1029/2001JA900056.

Singh, N., Schunk, R.W., 1984. Plasma response to the injection of an electron beam. Plasma Phys. Controlled Fusion 26, 859.

Singh, N., Thiemann, H., Schunk, R.W., 1987. Simulations of auroral plasma processes: Electric fields, waves and particles. Planet. Space Science 35, 353–395. https://doi.org/10.1016/0032-0633(87)90162-0.

Singh, S.V., Devanandhan, S., Lakhina, G.S., Bharuthram, R., 2013. Effect of ion temperature on ion-acoustic solitary waves in a magnetized plasma in presence of superthermal electrons. Phys. Plasmas 20, 012306. https://doi.org/10.1063/1.4776710.

Singh, S.V., Lakhina, G.S., 2001. Generation of electron-acoustic waves in the magnetosphere. Planet. Space Sci. 49, 107–114. https://doi.org/10.1016/S0032-0633(00)00126-4.

Singh, S.V., Lakhina, G.S., 2004. Electron acoustic solitary waves with non-thermal distribution of electrons. Nonlin. Process. Geophys. 11, 275–279, URL: https://hal.archives-ouvertes.fr/hal-00302331.

Singh, S.V., Lakhina, G.S., Bharuthram, R., Pillay, S.R., 2011. Electrostatic solitary structures in presence of non-thermal electrons and a warm electron beam on the auroral field lines. Phys. Plasmas 18, 122306. https://doi.org/10.1063/1.3671955.

Singh, S.V., Reddy, R.V., Lakhina, G.S., 2001b. Broadband electrostatic noise due to nonlinear electron-acoustic waves. Adv. Space Res. 28, 1643–1648. https://doi.org/10.1016/S0273-1177(01)00479-3.

Sitnov, M., Birn, J., Ferdousi, B., Gordeev, E., Khotyaintsev, Y., Merkin, V., et al., 2019. Explosive magnetotail activity. Space Sci. Rev. 215, 31. https://doi.org/10.1007/s11214-019-0599-5.

Tagare, S.G., Singh, S.V., Reddy, R.V., Lakhina, G.S., 2004. Electron acoustic solitons in the earth's magnetotail. Nonlin. Process. Geophys. 11, 215–218, URL: https://hal.archives-ouvertes.fr/hal-00302317.

Temerin, M., Cerny, K., Lotko, W., Mozer, F.S., 1982. Observations of double layers and solitary waves in the auroral plasma. Phys. Rev. Lett. 48, 1175–1179. https://doi.org/10.1103/PhysRevLett.48.1175.

Tsurutani, B.T., Arballo, J.K., Lakhina, G.S., Ho, C.M., Buti, B., Pickett, J.S., Gurnett, D.A., 1998. Plasma waves in the dayside polar cap boundary layer: Bipolar and monopolar electric pulses and whistler mode waves. Geophys. Res. Lett. 25, 4117–4120. https://doi.org/10.1029/1998GL900114.

Ur-Rehman, H., Mahmood, S., Ur-Rehman, A., 2014. Compressive and rarefactive ion-acoustic solitons in a magnetized two ion component plasma. Phys. Scripta 89, 105605. https://doi.org/10.1088/0031-8949/89/10/105605.

Vasyliunas, V.M., 1975. Interplanetary magnetic field and the auroral zones. Rev. Geophys. 13, 303–336. https://doi.org/10.1029/RG013i001p00303.

Verheest, F., Hellberg, M.A., 2021. Fast and slow beam mode ion-acoustic solitons in plasmas with counterstreaming cold protons. Phys. Scr. 96, 00. https://doi.org/10.1088/1402-4896/abde0d.

Wang, R., Lu, Q., Khotyaintsev, Y.V., Volwerk, M., Du, A., & Nakamura, e. a., R. (2014). Observation of double layer in the separatrix region during magnetic reconnection. Geophysical Research Letters, 41, 4851–4858. doi:10.1002/2014GL061157.

Yamada, M., Kulsrud, R., Ji, H., 2010. Magnetic reconnection. Rev. Mod. Phys. 82, 603–664. https://doi.org/10.1103/RevModPhys.82.603.

Yang, J., Cao, J.B., Fu, H.S., Wang, T.Y., Liu, W.L., Yao, Z.H., 2017. Broadband high-frequency waves detected at dipolarization fronts. Journal of Geophysical Research: Space Physics 122, 4299–4307. https://doi.org/10.1002/2016JA023465.

Zhao, M.J., Fu, H.S., Liu, C.M., Chen, Z.Z., Xu, Y., Giles, B.L., Burch, J. L., 2019. Energy range of electron rolling-pin distribution behind dipolarization front. Geophys. Res. Lett. 46, 2390–2398. https://doi.org/10.1029/2019GL082100.

Zhou, X.-Z., Runov, A., Angelopoulos, V., A.V., A., & Birn, J. (2018). On the acceleration and anisotropy of ions within magnetotail dipolarizing flux bundles. J. Geophys. Res.: Space Physics, 123, 429–442. doi:10.1002/2017JA024901.